*energies*

MDPI

*Article*

# Improved Model Predictive Direct Power Control for Parallel Distributed Generation in Grid-Tied Microgrids

**Muhammad Zubair Asif Bhatti [1], Abubakar Siddique [1], Waseem Aslam [2,*], Shahid Atiq [1] and Hussain Sarwar Khan [3]**

[1] Department of Electrical Engineering, Khwaja Fareed University of Engineering and Information Technology (KFUEIT), Rahim Yar Khan 64200, Pakistan
[2] Department of Electrical Engineering, University of Sargodha (UOS), Sargodha 40100, Pakistan
[3] Department of Electrical Engineering, University of Vaasa, 65200 Vaasa, Finland
* Correspondence: wasimevergreen@yahoo.com or waseem.aslam@uos.edu.pk

**Abstract:** This research proposes an improved finite control set direct power model predictive control method (FCS-DPMPC) for grid-tie distributed generation (DG). FCS-DPMPC predicts the system outcomes using the system model. During the next sampling time, a voltage vector is defined using the cost function to minimize the power ripple, consequently allowing flexibility for power regulation. Furthermore, the impact of implementing a one-step delay is studied and compensated through a model forecast pattern. In addition, a new two-step horizon technique has been developed to minimize switching frequency and computation burden. Simulation results for single DG and parallel operated DGs in a grid-tie manner confirm the effectiveness of the suggested control strategy, which signifies that this is an appropriate approach for distributed generation in microgrids.

**Keywords:** distributed generation (DG); power regulation (PR); renewable energy sources (RES); model predictive control (MPC); switching frequency reduction (SFR)



**Citation:** Bhatti, M.Z.A.; Siddique, A.; Aslam, W.; Atiq, S.; Khan, H.S. Improved Model Predictive Direct Power Control for Parallel Distributed Generation in Grid-Tied Microgrids. *Energies* **2023**, *16*, 1441. https://doi.org/10.3390/en16031441

Academic Editor: Ikhlaq Hussain

Received: 21 December 2022
Revised: 20 January 2023
Accepted: 26 January 2023
Published: 1 February 2023



## 1. Introduction

At present, environment-friendly distributed generation (DG) units (wave, photovoltaic, wind, and others) are rapidly developing as a result of the expanding need for power and the need to restrict the emission of ozone-depleting substances from conventional petroleum-based power plants [1–3].To acquire additional capability and control flexibility that prompts power quality and system reliability, DGs are coordinated with a common dc or ac bus via a storage system to develop a microgrid [4,5].

Due to the increase in the use of DG, bidirectional power flow was raised as an imperative issue for power system control and management. Microgrids (MGs) are an efficient implementation to improve power system reliability and quality [6]. Generally, Microgrids are characterized as 'an interconnected system of energy which consists of distributed generators and many loads as a single, independent of connected either in "Grid-Tie" or "Islanded" mode from the utility grid' [7]. A microgrid can be denoted by small power sources and electrical loads as shown in Figure 1. The micro sources, network parameters, loads, and control typologies in different microgrids are different. Small-signal stability, transient stability, and voltage stability are the three types of stability problems in a microgrid. The causes of every stability problem are shown in Figure 2.

Power system stability is a provoking job because of different load demands. In this scenario, microgrids ought to utilize and control to give active and reactive powers remuneration for stabilization of the main energy system in terms of system voltage and frequency [8]. In this manner, the power converter of the DG unit is needed to perform more appropriately and efficiently to keep dynamic stability and high-power quality.

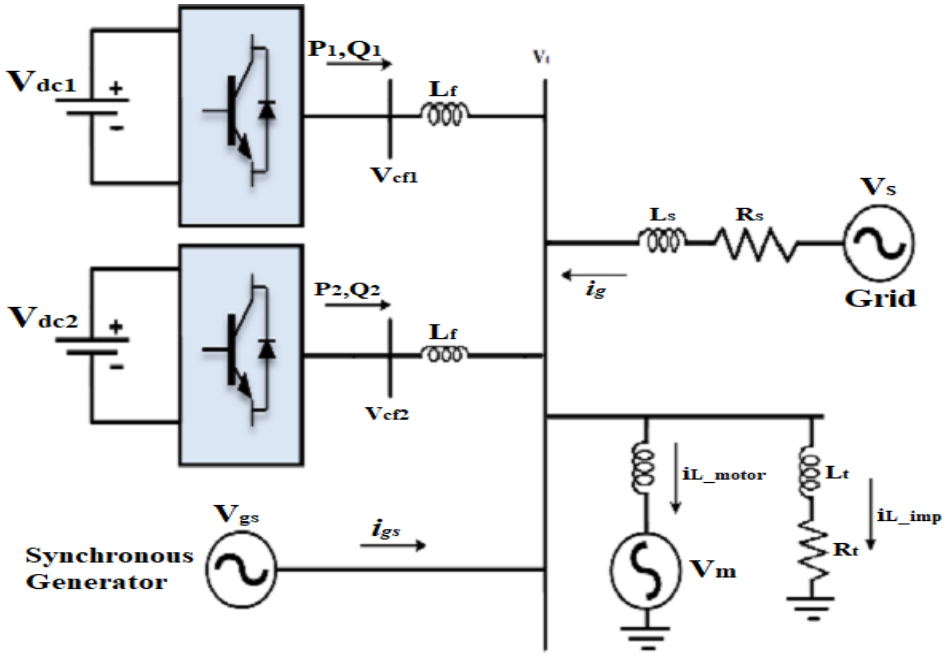


**Figure 1.** Microgrid with distributed generators and electrical loads.

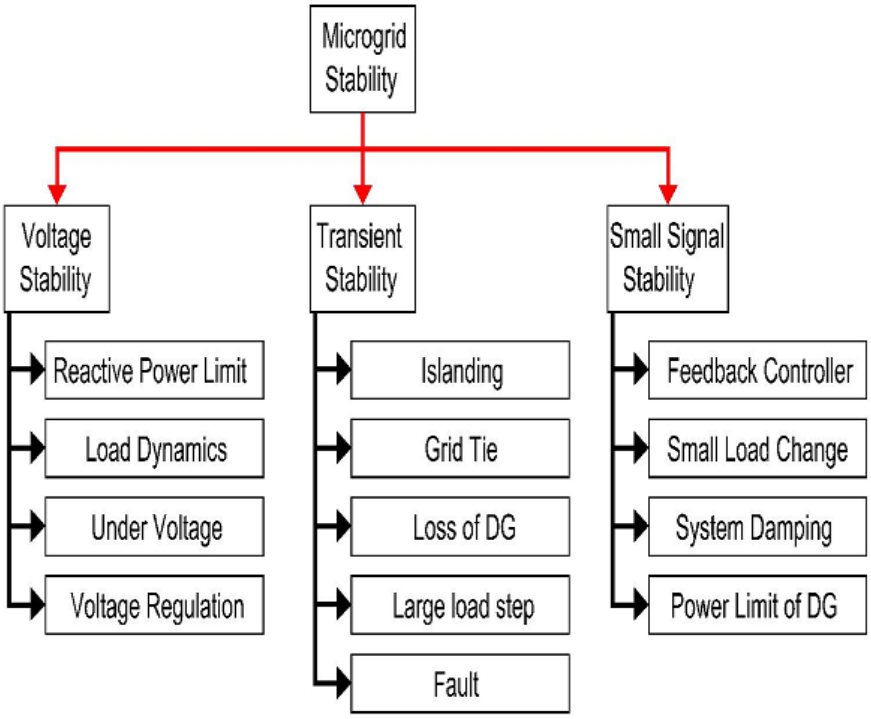


**Figure 2.** Issues of stability in MG and their reasons.

For grid-connected inverters, various control methods are used today. One of the most well-known is direct power control (DPC). Traditional switching-based DPC (SDPC) has been generally utilized because of its benefits such as straightforwardness, robustness, and magnificent performance [9]. Afterward, many further improved DPC techniques were created to perform better [10–12].

Model predictive control (MPC) is a viable option for power converter operation because it provides a flexible control pattern that permits the system nonlinearities and constraint inclusion. The present states and control action are employed in this control to forecast the behavior of the system using a system model and to choose the best switching

states, a cost function is utilized as a principle [13]. MPC control goals might change significantly depending on the application. For rectifiers, the control goals are active power and reactive power [14]; for inverters, the control goals are reducing the large current ripples and common-mode voltage (CMV) magnitude [15]; for permanent magnet synchronous motors, the control goal is torque control [16]; and in electrical networks even when the system voltage is not ideal, the control goal is dynamic convergence of dc bus voltage to the nominal reference voltage [17], improving frequency regulation for microgrid [18], and the voltage or current control in inverters [19–22].

The MPC schemes can be distributed in three categories: (1) DBC—deadbeat control [23,24]; (2) CCS-MPC—continuous-control-set model predictive control [25,26]; and (3) FCS-MPC—finite-control-set model predictive control [27–30].

In the DBC scheme, the discrete-time framework model is used to trace down the reference voltage (RV), which is required to calculate the reference current/power during the next sample period. After that, the power converter utilizes a modulator to apply reference voltage (RV). DBC is uncomplicated, and its implementation is straightforward. Though DBC is designed with the framework model in consideration, it is sensitive to numerous mode parameters. CCS-MPC forecasts the future response of the controlled object based on its discrete model over the forecast horizon. Accordingly, an optimization function is utilized to acquire the best voltage vector to employ with the modulator. The limitations/nonlinearities of the object under control are easy to incorporate in CCS-MPC.

Finite-control-set MPC, also called direct MPC (DMPC), solves the optimization problem by utilizing the converter discrete-time model and a minimal set of switching vectors [27–30]. Hence, its computation burden is remarkably lesser than the CCS-MPC. In this approach, the entire DMPC algorithm is typically carried out online. Moreover, it is uncomplicated to include the nonlinearities and constraints/limitations of the framework controlled in the FCS-MPC design.

The current/power waveforms had more ripples even with a small sampling period as compared to the VOC approach with a modulation, despite having one voltage vector (VV) for each control duration. This issue may be addressed by increasing sample frequency or decreasing sampling duration, which will reduce ripples and improve FCS-MPC performance during the steady-state. This technique is increasing the cost of hardware. However, this technique enhances the FCS-MPC steady-state performance without decreasing sampling time which is essential. An overview of MPC schemes is detailed in Table 1.

**Table 1.** Overview of control schemes.

| | **Dead-Beat** | **CCS-MPC** | **FCS-MPC** |
|---|---|---|---|
| Theoretical background | Moderate | Strong | Strong |
| Stability analysis tools | Strong | Initial Results | Initial Results |
| Computational complexity | Average | High | High |
| Intuitive design | Average | High | High |
| Handling system constraints | No | Yes | Yes |
| Handling non-linearities | Yes | Yes | Yes |
| Parameter sensitivity | Average | Tunable | Tunable |
| Fault tolerance capability | No | Yes | Yes |
| Modulator | Required | Required | Not Required |
| Switching Frequency | Fixed | Fixed | Variable |

To improve the response of FCS-MPC in grid-tied power converters, in each sampling interval null and active vectors are implemented. However, current ripples continue to be greater compared to the linear controllers [31]. To resolve this issue, [32,33] introduced a multiple vector-based MPC with two active voltage vectors and a zero voltage vector. However, the proposed algorithms have a high computational burden. Moreover, the FCS-MPC concept is lost in these techniques [32,33] as an infinite number of VVs are used in the converter. Furthermore, the methods proposed in [32,33] are sensitive to mismatches or uncertainties in the parameters of the system model.

The FCS-MPC method does not use any kind of modulator, it uses the power converter's discrete nature. The conventional FCS-MPC forecasts all possible future performances by using a finite number of switching and choosing the most appropriate switching state to reach the control objectives using an already defined cost function [34,35]. Although in [36,37], there are significant ripple components in current waveforms, to improve the output current quality of conventional FCS-MPC, quite large passive filters are used. Furthermore, in a multi-level system with an increase in output voltage level, the number of possible switching states rises as well, resulting in the burden of extensive computation and long calculation time. Hence, a relatively higher switching frequency will cause more significant power loss. Therefore, the focus is to decrease the switching frequency in the power controller [38].

The following are the paper's primary contributions and salient features:

1. This work presents an improved finite control set direct power model predictive control (FCS-DPMPC) approach for grid-tied inverters based on the flexibility of the MPC method. A cost function is utilized to first lower the ripples in active and reactive powers.
2. In the digital implementation of the grid-tie system, a model predictive technique is formulated to compensate for a step delay. In addition, the switching frequency is reduced by developing two-step predictions (N = 2) so the losses of the inverter are minimized.
3. The simulation results show that the proposed control approach is proven to be competent.

The following is how this paper is structured: Section 2 describes the System Modeling. The proposed FCS-DPMPC controller in which flexible power regulation, compensation of implementation one-step delay, computational burden, reduction of switching frequency, and stability and performance is explained in Section 3. The simulation results for single DG in grid tie mode, parallel operation of DGs in grid-tie, reduction of switching frequency, stability and performance, and comparison between different techniques are described in Section 4. Finally, the paper's conclusion is presented in Section 5.

## 2. System Modelling

Figure 1 shows the GC-DG feeding the load. In this paper, focus is on the inverter. Inverters can switch between the following switching states:

$$S_i = 1(Upper\ side\ of\ bridge\ of\ phase\ i\ is\ "on"\ and\ lower\ side\ is\ "off")$$
$$S_i = 0\ (Upper\ side\ of\ bridge\ of\ phase\ i\ is\ "off"\ and\ lower\ side\ is\ "on")$$

The inverter has eight switching states: (0 0 0), (0 0 1), (0 1 0), (0 1 1), (1 0 0), (1 0 1), (1 1 0), and (1 1 1). The voltage of a three-phase two-level inverter is expressed as:

$$v_i = \frac{2}{3} v_{dc} e^{j(i-1)\pi/3}\ (i = 1 \ldots 6) \quad (1)$$

$$v_i = 0\ (i = 0, 7) \quad (2)$$

According to Kirchhoff's law, the state equations are represented as:

$$i_l = i_0 - i_g \quad (3)$$

$$i_c = i_f - i_0 \tag{4}$$

$$v_t = v_{pc} + v_f + i_f R_f \tag{5}$$

$i_l, i_c, i_f$, and $i_g$ are load current, capacitor current, filter current, and grid current. In Equation (5) $v_t$, $v_{pc}$, and $v_f$ are the output voltage of VSI, capacitor voltage at the point of common coupling (PCC), and filter voltage, respectively. To compute the CTSS model of the system, assuming that the system is balanced and has a sinusoidal wave of Voltage at PCC ($v_{pc}$), it should be written as:

$$v_{pc} = v_{pc,\alpha} + iv_{pc,\beta} \approx \ |v_{pc}|e^{-i\omega t} \tag{6}$$

Taking the explicit derivative of the above equation with respect to time, it becomes:

$$\frac{dv_{pc,\alpha}}{dt} = \omega v_{pc,\beta} \tag{7}$$

$$\frac{dv_{pc,\beta}}{dt} = -\omega v_{pc,\alpha} \tag{8}$$

$\omega = 2\pi f$ and $f$ is system frequency and can be determined by using PLL block in MATLAB simulation. The filter current equations are as:

$$\frac{di_{f,\alpha}}{dt} = \frac{1}{L_f}\left(v_{t_\alpha} - v_{pc,\alpha} - i_{f,\alpha}R_f\right) \tag{9}$$

$$\frac{di_{f,\alpha\beta}}{dt} = \frac{1}{L_f}\left(v_{t_\beta} - v_{pc,\beta} - i_{f,\beta}R_f\right) \tag{10}$$

## 3. Proposed FCS-DPMPC Controller

By using the FCS-DPMPC controller, DGs can regulate their power more flexibly, with a reduced inverter's switching frequency.

### *3.1. Flexible Power Regulation*

Active and reactive power are used as the state variables by the system to gain power regulation flexibility by DG. These should be gained from the design of the FCS-DPMPC controller for DG. A major challenge of this research is the development of an active power model.

GC-DG's active and reactive power are represented by the following state equations:

$$P = \frac{3}{2}\left(v_{pc,\alpha}i_{f,\alpha} + v_{pc,\beta}i_{f,\beta}\right) \tag{11}$$

$$Q = \frac{3}{2}\left(v_{pc,\beta}i_{f,\alpha} - v_{pc,\alpha}i_{f,\beta}\right) \tag{12}$$

By differentiating the equations of $P$ and $Q$ with respect to time, the following equations are obtained:

$$\frac{dP}{dt} = \frac{3}{2}\left(\frac{dv_{pc,\alpha}}{dt}i_{f,\alpha} + v_{pc,\alpha}\frac{di_{f,\alpha}}{dt} + \frac{dv_{pc,\beta}}{dt}i_{f,\beta} + \frac{di_{f,\beta}}{dt}v_{pc,\beta}\right) \tag{13}$$

$$\frac{dQ}{dt} = \frac{3}{2}\left(\frac{dv_{pc,\beta}}{dt}i_{f,\alpha} + v_{pc,\beta}\frac{di_{f,\alpha}}{dt} - \frac{dv_{pc,\alpha}}{dt}i_{f,\beta} - v_{pc,\alpha}\frac{di_{f,\beta}}{dt}\right) \tag{14}$$

Now, the equations for $\frac{dv_{pc,\alpha}}{dt}$, $\frac{di_{f,\alpha}}{dt}$, $\frac{dv_{pc,\beta}}{dt}$, and $\frac{di_{f,\beta}}{dt}$ are calculated from the computed CTSS model of the system by using Equations (9)–(12) and generalization.

$$\frac{dx}{dt} = A_g x + \frac{3}{2L_f} B_{1g} v_t - \frac{3}{2L_f} B_{2g} v_{pc} \tag{15}$$

where,

$$x = \begin{bmatrix} P \\ Q \end{bmatrix} \tag{16}$$

$$A_g = \begin{bmatrix} \frac{-R_f}{L_f} & -\omega \\ \omega & \frac{-R_f}{L_f} \end{bmatrix} \tag{17}$$

$$B_{1g} = \begin{bmatrix} v_{pc,\alpha} & v_{pc,\beta} \\ v_{pc,\beta} & -v_{pc,\alpha} \end{bmatrix} \tag{18}$$

$$B_{2g} = \begin{bmatrix} v_{pc,\alpha} & v_{pc,\beta} \\ 0 & 0 \end{bmatrix} \tag{19}$$

Discrete-time state space model (DT-SSM) is used for prediction by converting the CTSS model to DT-SSM, for this, the Euler forward approximation method is used which is described as:

$$\frac{dx}{dt} = \frac{x(t_k+1)' - x(t_k)}{T_s} \tag{20}$$

so,

$$x(t_k+1)' = A_{g1}\, x(t_k) + B_{g1} V_t(t_k) + B_{g2} i_0(t_k) \tag{21}$$

where,

$$A_{g1} = e^{A_g T_s} \tag{22}$$

$$B_{g1} = \int_0^{T_s} e^{A_g \tau}\, B_{1g} d_\tau \tag{23}$$

$$B_{g2} = \int_0^{T_s} e^{A_g \tau}\, B_{2g} d_\tau \tag{24}$$

If the sampling time is very small, then the exponential matrix is approximated as:

$$e^{A_g T_s} \approx 1 + A_g T_s \tag{25}$$

Based on above equations, $P(t_k+1)'$ and $Q(t_k+1)'$ are find through the following equations:

$$P(t_k+1)' = P(t_k) + T_s \left[ \frac{-R_f}{L_f} P(t_k) - \omega Q(t_k) + \frac{3}{2L_f} \left( v_{pc,\alpha}(t_k) v_{t_\alpha}(t_k) + v_{pc,\beta}(t_k) v_{t_\beta}(t_k) \right) - \frac{3}{2L_f} \left( {v_{pc,\alpha}}^2(t_k) + {v_{pc,\beta}}^2(t_k) \right) \right] \tag{26}$$

$$Q(t_k+1)' = Q(t_k) + T_s \left[ \frac{-R_f}{L_f} Q(t_k) + \omega P(t_k) + \frac{3}{2L_f} \left( v_{pc,\alpha}(t_k) v_{t_\alpha}(t_k) + v_{pc,\beta}(t_k) v_{t_\beta}(t_k) \right) \right] \tag{27}$$

In the proposed FCS-DPMPC controller, these equations are used as the predictive model. The essential properties of the FCS-DPMPC strategy are clearly illustrated in Figure 3. Using the DT-SSM of the system, all the possible system conversions $x(t_k+1)'$ can be forecasted for the control actions of N (N = 1, 2, 3, . . . , n), and for each control action, the transition which is closer to reference x* is selected. In a desire to gain flexible power regulation, the FCS-DPMPC control strategy for GC-DG is shown in Figure 4.

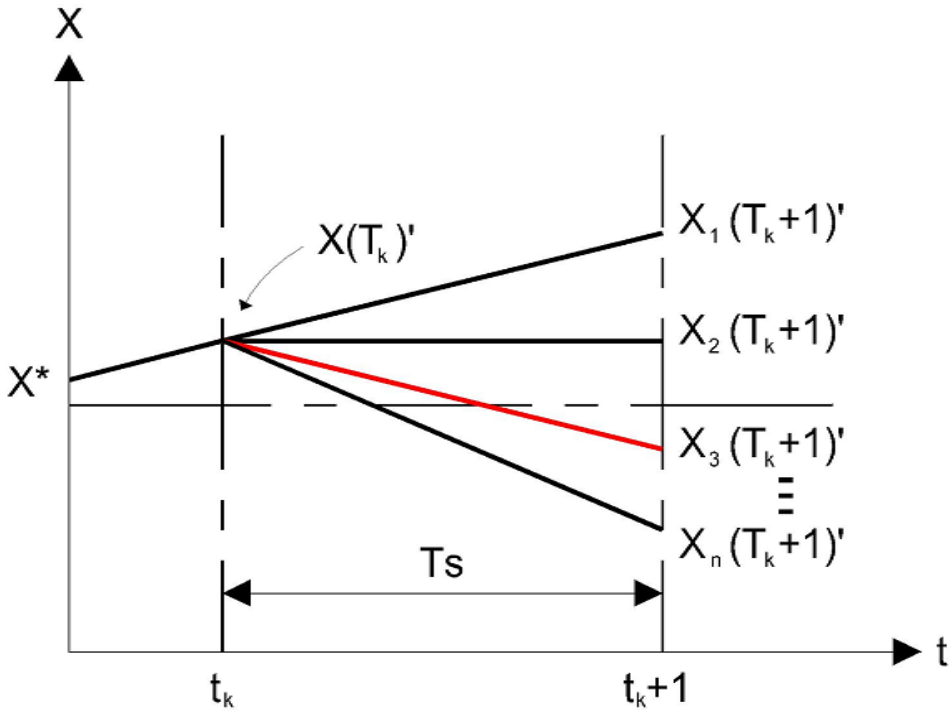


**Figure 3.** Voltage vector evaluation and selection for DPM.

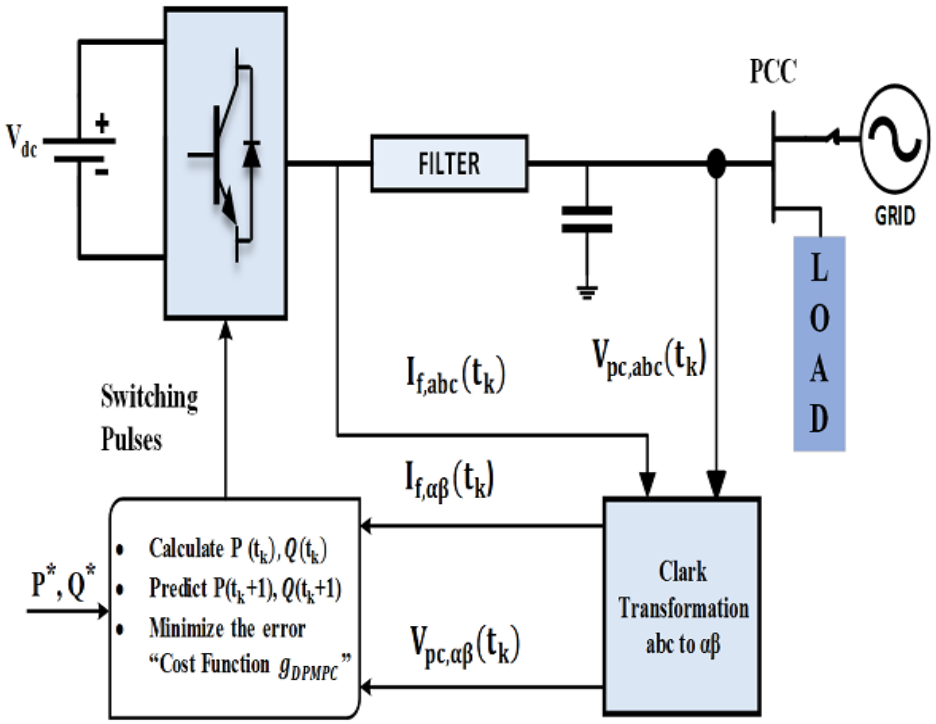


**Figure 4.** Block diagram of FCS−DPMPC.

A cost function is used to choose the best transition by comparing all the forecasted powers. To minimize the power error, the following cost function is utilized.

$$g_{DPMPC} = (P^*(t_k+1)' - P(t_k+1)')^2 + (Q^*(t_k+1)' - Q(t_k+1)')^2 \quad (28)$$

where $P^*(t_k+1)'$ is the reference active power and $Q^*(t_k+1)'$ is a reference to the reactive power. To decrease the power error above, cost function is selected so that the GC-DG can insert any quantity of active and reactive power within its extent.

### *3.2. Compensation for Implementational One-Step Delay*

In real-world applications, digital signal processors (DSPs) have a one-step delay due to the switching state calculated in the previous phase being implemented at the start of the following control step [39,40]. For a detailed study of the one-step delay, Figure 5 describes the control algorithm execution in the DSP in which control variable $x(t_k)$ is sampled at t = $t_1$, analog to digital converter (ADC) procedure is completed at t = $t_2$, and computation of voltage vector is completed at t = $t_3$. However, we cannot implement it until the next sampling period at t = $t_4$. After determining the voltage vector $Vi(t_k)$ and using $x(t_k)$ and $x^*$ at t = $t_3$, it cannot be implemented until the instance of $(t_k+1)$. Although, the variables at $(t_k+1)$ are changed to $x(t_k+1)'$ and are mainly diverse from $x(t_k)$ due to the implementation of $Vi(t_k-1)$. Therefore, the obtained vector implemented at $(t_k+1)$ based on $x(t_k)$ might not be the finest. Hence, $x(t_k+1)'$ should be implemented to determine the voltage of interest $Vi(t_k)$ which will reduce the error at $(t_k+2)$ with respect to the reference $x^*$.

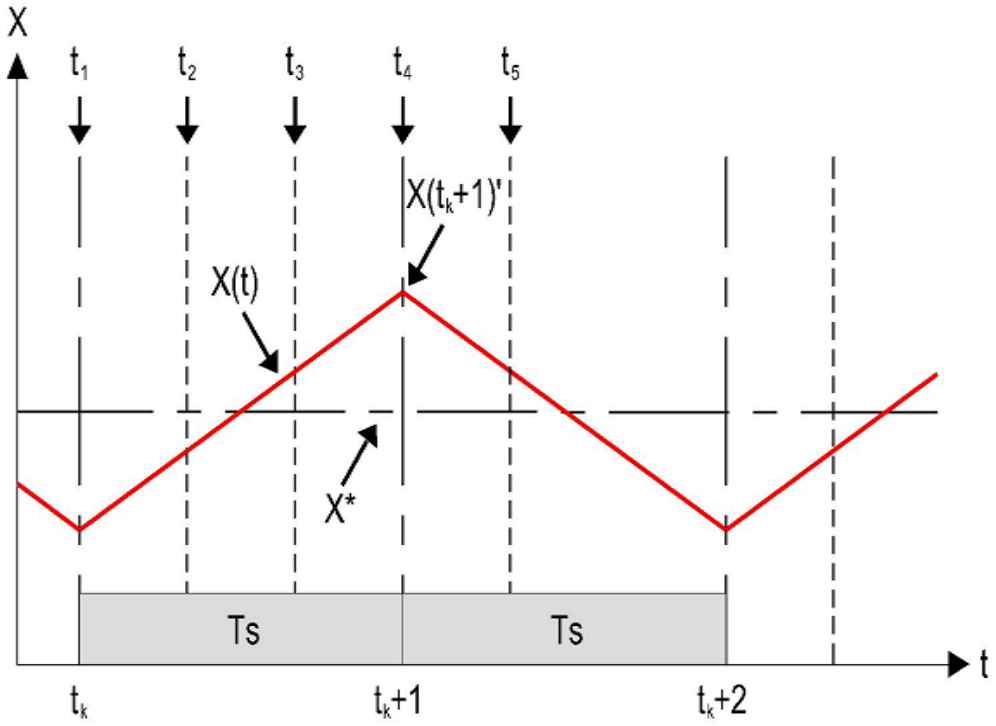


**Figure 5.** Processing data in a DSP.

In this paper, for the compensation of a one-step delay, a two-step prediction scheme is formed by using the MPC strategy. Firstly, $P(t_k+1)'$ and $Q(t_k+1)'$ are obtained using Equations (26) and (27). Then, $P(t_k+2)'$ and $Q(t_k+2)'$ are predicted by using $P(t_k+1)'$, $Q(t_k+1)'$, and $Vi(t_k)$ as the input. Accordingly, the cost function is revised to:

$$g_{DPMPC} = (P^*(t_k+2)' - P(t_k+2)')^2 + (Q^*(t_k+2)' - Q(t_k+2)')^2 \quad (29)$$

Equation (29) expresses the implemented cost function with horizon N = 2, taking the different vectors throughout the sampling duration, where $P^*(t_k+2)'$ is the reference active power and $Q^*(t_k+2)'$ is the reference reactive power.

### *3.3. Computational Burden*

The prediction horizon N = 1 is shown in Figure 6A in which eight voltage vectors are computed during a one-step horizon. By extending the horizon to N = 2 as shown in Figure 6B, throughout the first sampling duration, one voltage vector is implemented, and an additional vector is used for the second sampling period. In the case of N = 2, the total possible sequence of two voltage vectors is $7^2$. This means a total of 49 possible sequences should be computed. This will result in an experimental implementation problem because it needs a huge number of calculations.

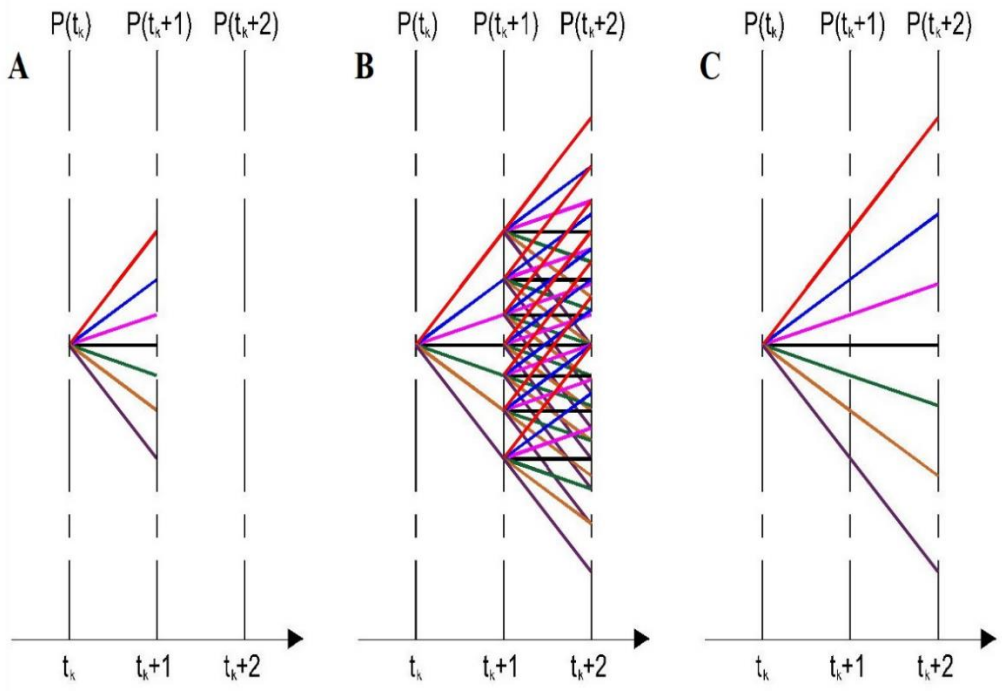


**Figure 6.** Representation of the Forecast scheme, (**A**) for horizon N = 1, (**B**) for horizon N = 2 taking the different vectors throughout sampling duration, and (**C**) N = 2 taking the similar vectors throughout two sampling duration.

### *3.4. Reduction of Switching Frequency*

In DG, to achieve small power losses, the switching frequency should be low, such that a low computational burden and high efficiency can be obtained. Here, a simplified two-step forecast is implemented to decrease the computational burden. The same voltage vector is judged throughout the sampling time, resulting in only seven voltage vectors estimated throughout the two-step forecast, as presented in Figure 6.

This technique gives a similar result with less switching frequency rather than implementing all voltage vectors [14]. The modified cost function is:

$$g_{DPMPC} = \left[\left(P^* - P(t_k+1)'\right)^2 + \left(Q^* - Q(t_k+1)'\right)^2\right] + \left[\left(P^* - P(t_k+2)'\right)^2 + \left(Q^* - Q(t_k+2)'\right)^2\right] \quad (30)$$

Equation (30) summarizes the desired cost function of modified horizon N = 2, taking similar vectors throughout the two sampling duration, where $P^*$ is the reference active power and $Q^*$ is the reference reactive power. This approach of two-step prediction decreases the switching frequency, so the power ripples. The algorithm for the proposed modified FCS-DPMPC is shown in Figure 7.

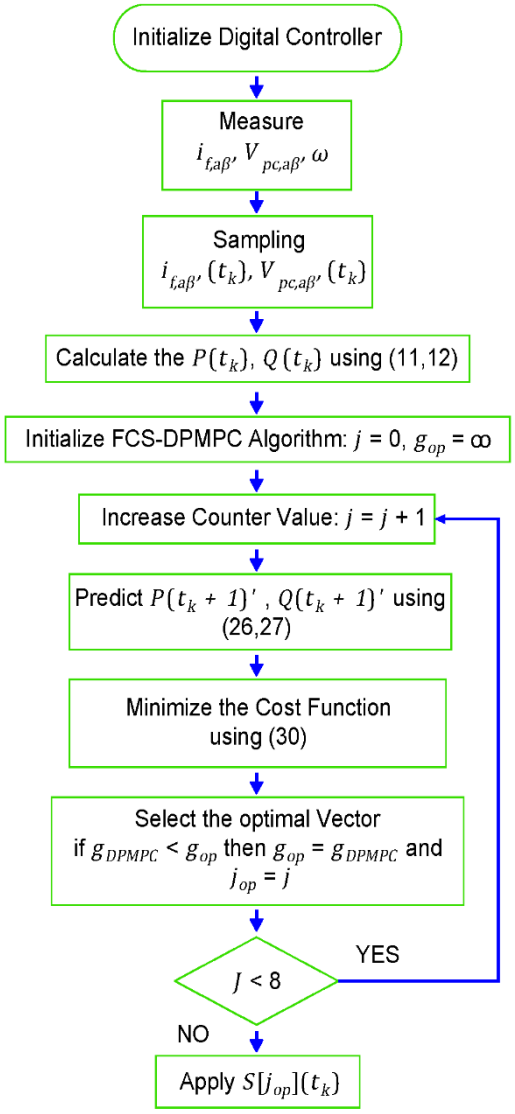


**Figure 7.** Algorithm for the proposed modified FCS-DPMPC.

### *3.5. Stability and Performance*

Every control algorithm application requires an assessment of the performance and stability in a closed-loop operation. Output variables (i.e., voltages, currents, and power) tend to diverge from the value of set-points in closed-loop control of power converters. The MPC's closed-loop stability is typically examined using the Lyapunov stability theory. While the infinite-horizon MPC ensures stability, the closed-loop MPC is not always stable with limited prediction horizons [41]. Due to the non-linear character of FCS-MPC approaches, they cannot depend on the well-established classical methodologies used for linear systems. A closed-loop stability study of FCS-MPC is challenging unless complicated mathematics is applied [42]. Due to a lack of analytical tools for evaluating the performance of MPC for power converters, lengthy simulations or experiments were used to test the algorithm's performance [43]. A new strategy is required in this area. However, the performance of MPC in real-time scenarios is very good. Table 2 summarizes the stability studies in the domain of MPC for power converters.

**Table 2.** Literature review of state-of-the-art stability and performance validation of FCS-MPC.

| Ref. | Interest | Technique | Pros | Cons | Verified Performance | Verified Stability |
|---|---|---|---|---|---|---|
| [44] | 4-leg VSC | Multiple sim., parameter sweep | Quick, simple cost function design | Closed loop stability is not well-defined, and is not a certified approach | Yes | No |
| [45] | MMC | Multiple sim., parameter sweep | Quick, simple cost function design | Closed loop stability is not well-defined, and is not a certified approach | Yes | No |
| [46] | 2L-VSC | Multiple exp., benchmarking | Quick, simple cost function design | Closed loop stability is not well-defined, and is not a certified approach | Yes | No |
| [47] | 2L-VSC | Lyapunov stability theory | Proved method | Only stability of the neighborhood of system reference is sure, complex cost-function design | Yes | No |
| [48] | DC-DC | Lyapunov stability theory | Proved method | Only stability of the neighborhood of system reference is sure, complex cost-function design | Yes | Yes |
| [49] | MCC | Lyapunov stability theory | Proved method | Only stability of the neighborhood of system reference is sure, complex cost-function design | Yes | Yes |
| [50] | AFE | Lyapunov stability theory | Proved method | Not a conventional FCS, complex cost-function design | No | Yes |

Statistical model checking is a well-known technique that helps in resolving problems that are intractable by conventional formal techniques used in embedded vehicles, sensor networks, and communication systems [51,52]. Numerous simulations, experiments, and analytical analyses using the Lyapunov stability criterion are the three methods used to assess stability and performance. The method of performance verification will be the focus of our attention. Running many simulations appears to be the easiest way, but it is also the most time demanding. Further on, the procedure's reliability is absent. Since there is no assurance that a finite set of tests will cover entire potential circumstances, errors may go unnoticed. Looking at the physical system characteristics, we can see that certain components have probabilistic behavior, such as reference values for active and reactive power generation. Representing them as fixed components is not beneficial if we wish to verify the execution of the control algorithm during transients. As a result, to assure a system's complete correctness, we must employ formal methods.

Formal methods employ mathematical techniques to verify system behavior in all possible contexts and Statistical Model Checking (SMC) is an extension of one such approach. The system will be simulated for a finite number of times using this method. The simulated samples are utilized for hypothesis testing, which involves determining if the samples give statistical evidence that the set hypothesis is correct [53]. Two sorts of tests may be performed: verifying if the probability of satisfying the condition is under a certain threshold and estimating this probability. Hypothesis testing techniques are employed for the first testing and Monte Carlo simulation procedures are utilized for the latter. The Monte Carlo techniques have been improved to address the issues of predicting low probability and unusual events.

## 4. Numerical Simulation

To validate the performance of the proposed FCS-DPMPC, different cases are designed to analyze their response under different conditions by using MATLAB/Simulink, and system parameters are described in Table 3.

**Table 3.** System Parameters.

| Parameters | Symbol | Values |
|---|---|---|
| DC-link voltage | $V_{dc}$ | 1000 V |
| Filter Inductor | $L_f$ | 2 mH |
| Filter resistor | $R_f$ | 0.04 Ω |
| Damping resistor | $R_c$ | 0.94 Ω |
| Frequency | $f$ | 60 Hz |
| Load | $P, Q$ | 18 kW, 7 kVar |
| Grid parameters | $R_g, L_g$ | 0.0023 Ω, 12 µH |
| Grid Voltage | $V_g$ | 380 V |

The voltage and frequency of the system are stable in the grid-connected mode and follow the main grid references. So, there is no need to use the voltage and frequency controller. In GC mode, the PQ controller is used for accurate power sharing because in this case DG is used as a grid-feeding inverter and current is injected into the grid to fulfill the load requirements.

### *4.1. Single DG in Grid Tie Mode*

A single DG is connected to the grid through a common bus. In this case, FCS-DPMPC delivers flexible power between DG and gird. The FCS-DPMPC technique is tested for both two-step horizon prediction with cost function Equation (29) and the modified two−step horizon prediction with cost function Equation (30). The output voltage, current, and power injection performance are shown in Figure 8.

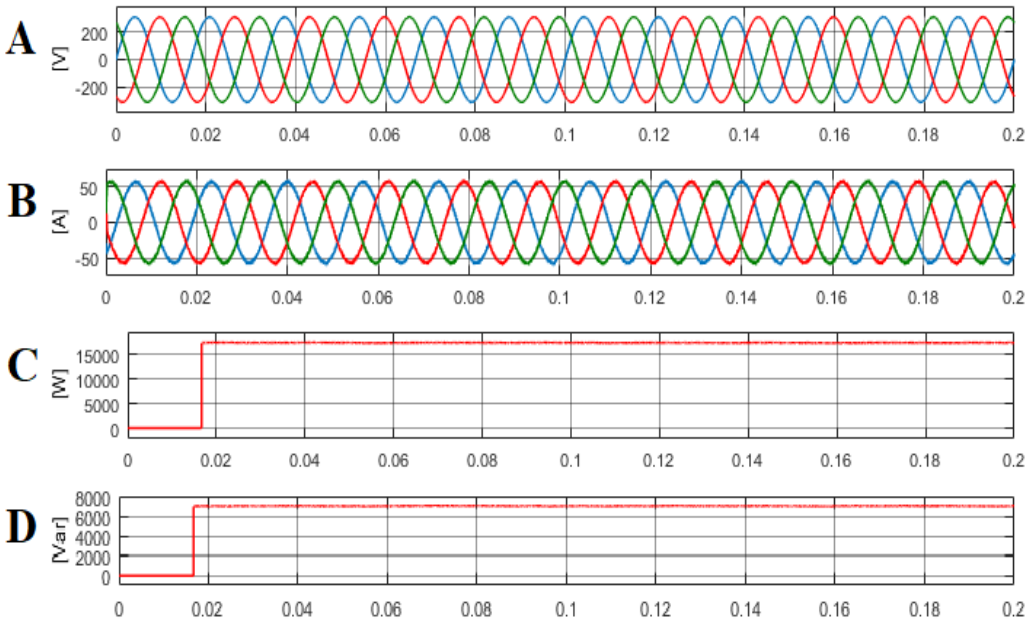


**Figure 8.** Representation simulation validation of the proposed control strategy with Linear Load. (**A**) Voltage waveform fundamental voltage amplitude: 318 V, (**B**) load current waveform, (**C**) active power provided by VSC in "W", and (**D**) reactive power provided by VSC in (Var).

Figure 8A,B presents the output voltage and current waveforms, and Figure 8C,D presents the DG's active and reactive power injections. The current injected by grid-connected DG into the common bus is seen to be very sinusoidal, with a total harmonic

distortion (THD) of only 0.96 percent for two-step horizon prediction and 1.01 percent for modified two-step horizon prediction. Figures 9 and 10 represent the %THD of current for the two-step horizon prediction and modified two-step horizon prediction. Waveforms are stable, showing the proposed controller's robustness under linear load.

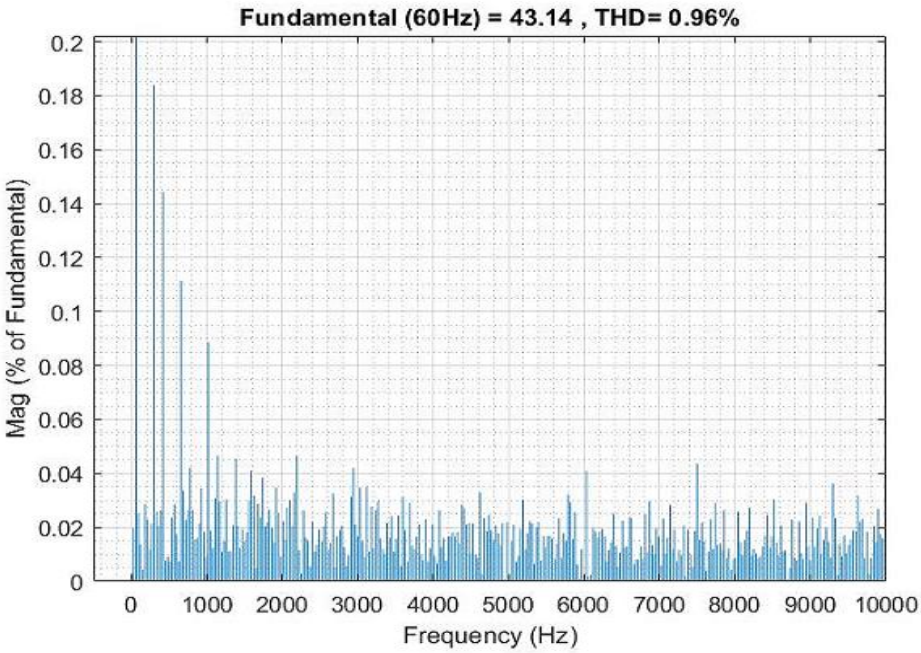


**Figure 9.** %THD of current for the two-step horizon prediction for single DG connected in grid-connected mode.

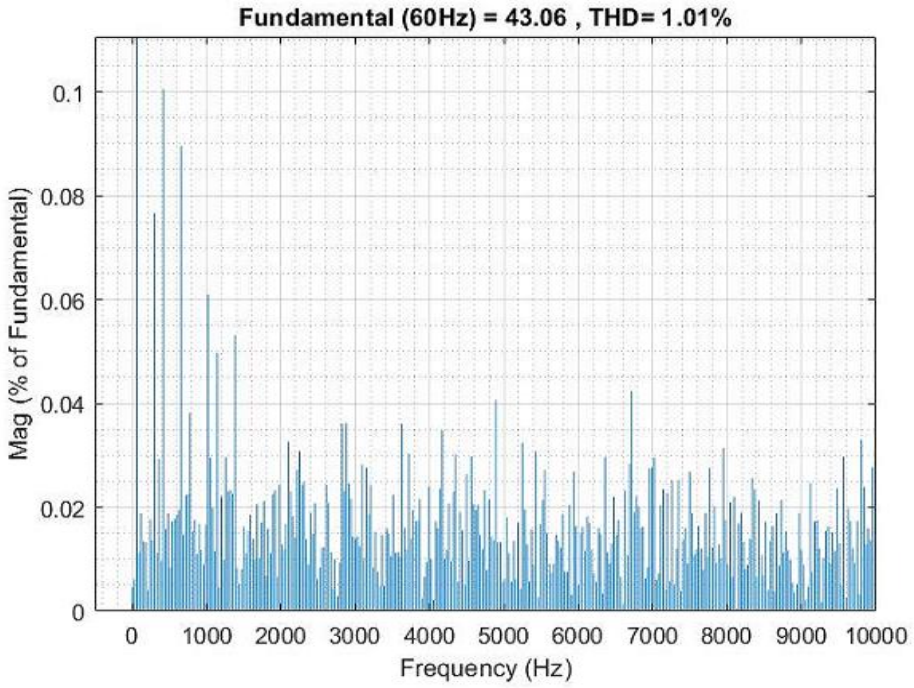


**Figure 10.** % THD of current for the modified two-step horizon prediction for a single DG connected in grid-connected mode.

Step Change in P and Q Reference Values for Single DG

In this case, the VSC is in grid feeding mode and at the instant t = 0.1 the reference value of P is changed from 18 kW to 28 kW, and Q is changed from 7KVAR to 10KVAR.

Figure 11 shows the increase in current, active power, and reactive power to fulfill the new demand and it can be seen that the time taken by the power to stabilize at the new reference is less than 0.02 s.

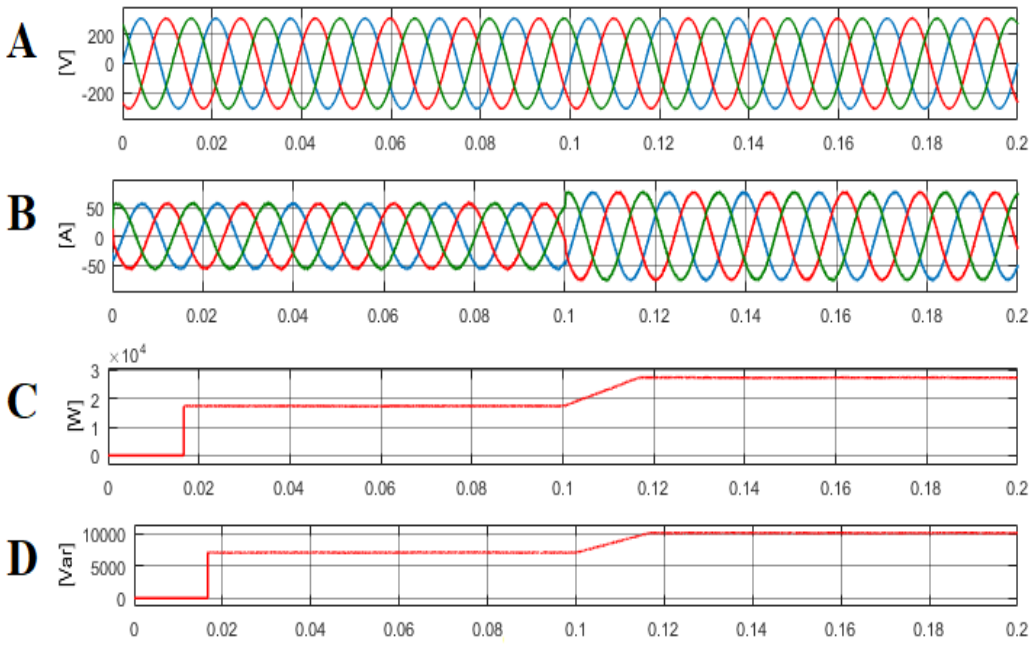


**Figure 11.** Simulation validation of proposed control strategy with the change of reference (**A**) Voltage waveform fundamental voltage amplitude: 318 V (**B**) load current waveform (**C**) Active power provided by VSC in "W". (**D**) Reactive power provided by VSC in "VAR".

### *4.2. Parallel Operation of DGs in Grid Tie Mode*

In this case, the FCS-DPMPC controller is designed for parallel grid-connected DGs. Figures 12–16 show the obtained results for the parallel-connected DGs in the grid tie to fulfill the demand. Figure 12A,B shows the obtained results for the output voltage and current of DG1 in the parallel-connected mode of operation, and Figure 12A,B shows the output voltage and current of DG2 in the parallel-connected mode of operation. Clearly, it can be seen that both the voltage and current for both DGs are sinusoidal and balanced in phase.

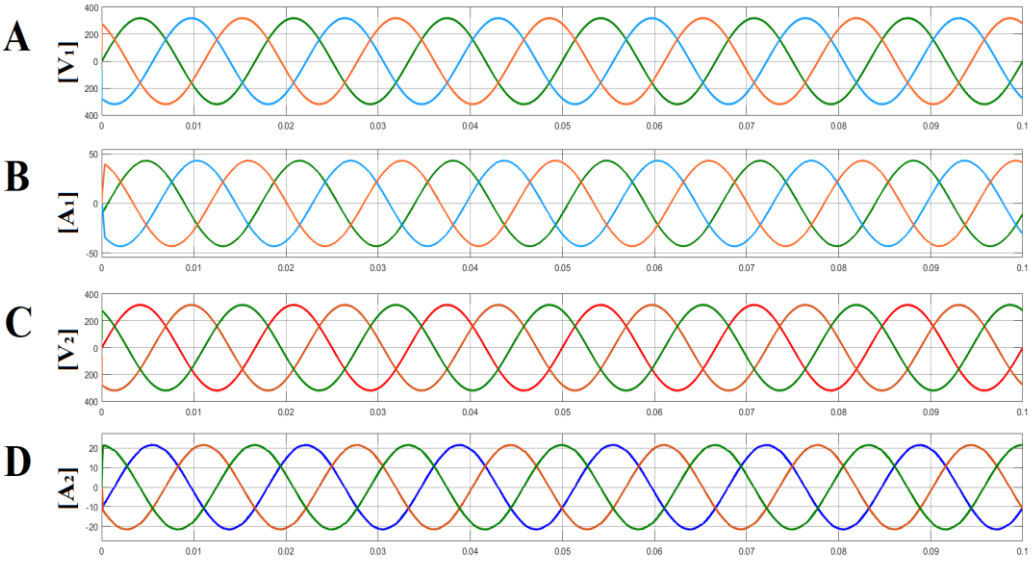


**Figure 12.** The waveform of output voltages and currents (**A**,**B**) of DG1 and (**C**,**D**) of DG2 in GC mode.

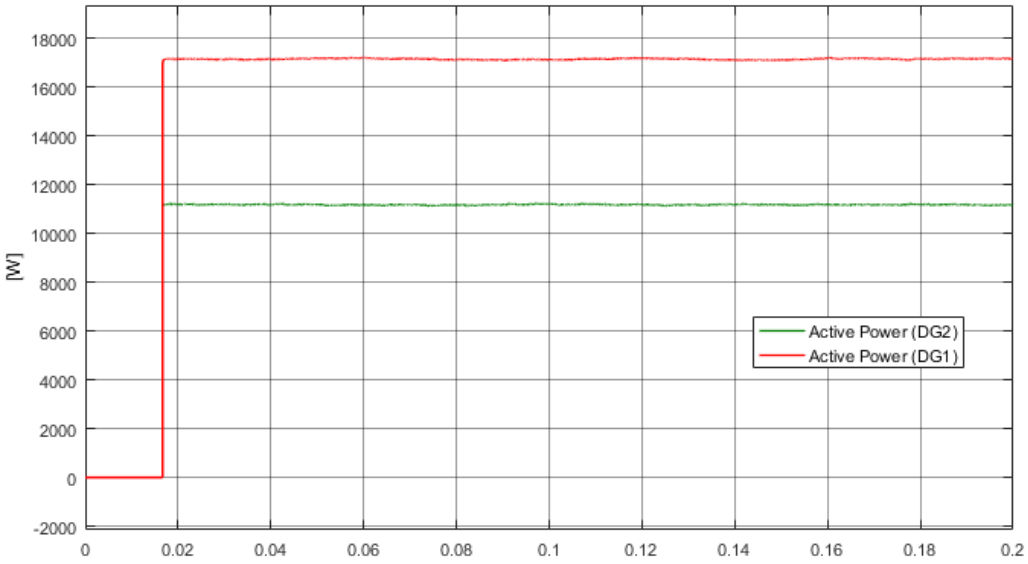


**Figure 13.** The waveform of the active power of DGs for parallel operation in GC mode.

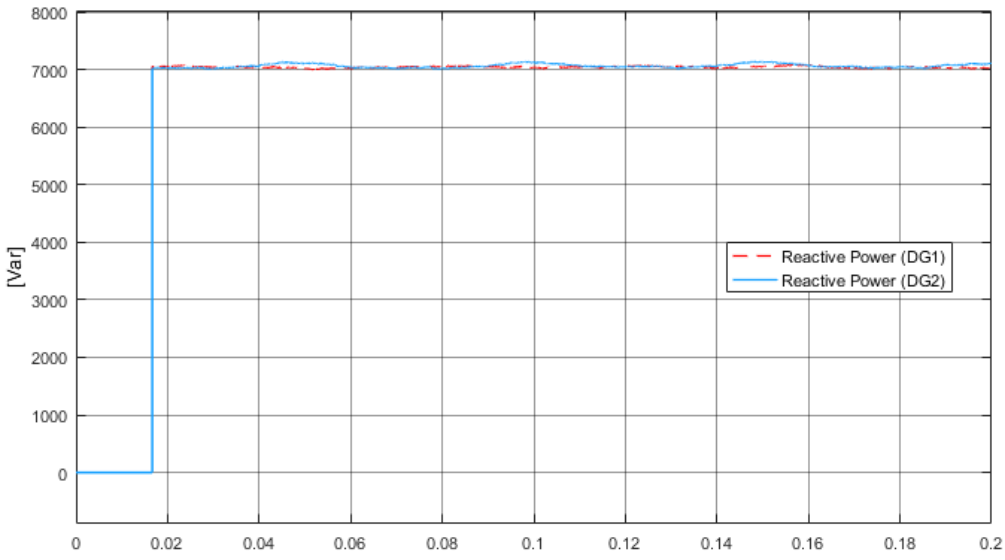


**Figure 14.** The waveform of the reactive power of DGs for parallel operation in GC mode.

Figure 13 shows the obtained results for the active power of individual DG and Figure 14 shows the reactive power of individual DG in the parallel-connected mode of operation.

Moreover, Figure 15 shows the obtained results of total harmonic distortion (THD) for two-step horizon prediction which is 1.01 percent. Figure 16 shows the obtained results of total harmonic distortion (THD) for modified two-step horizon prediction for parallel-connected DGs in the grid tie to fulfill the demand which is 1.06 percent and slightly higher than the THD of two-step horizon prediction.

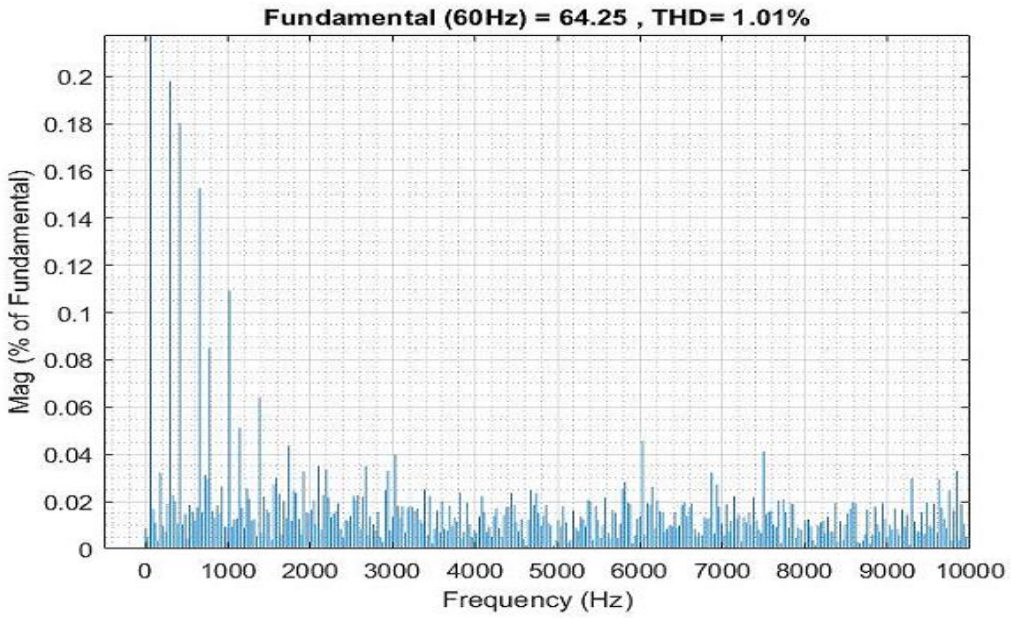


**Figure 15.** %THD of current for the two-step horizon prediction for parallel-connected DGs in grid-connected mode.

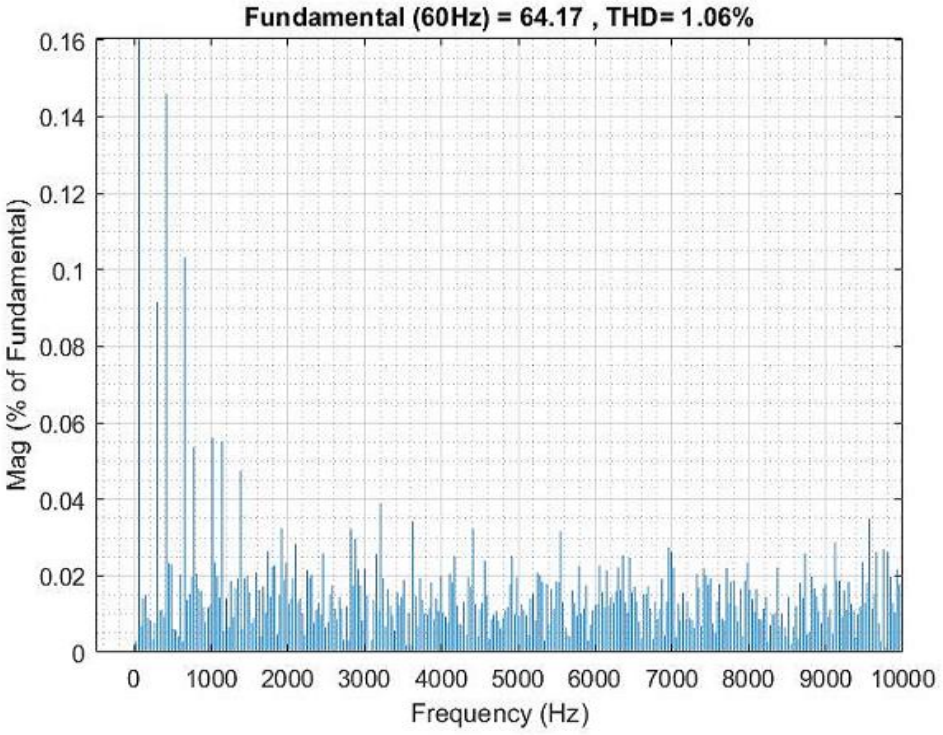


**Figure 16.** %THD of current for the two-step horizon prediction for parallel-connected DGs in grid-connected mode.

### *4.3. Switching Frequency Reduction*

The approach of the modified two-step prediction technique reduces the switching frequency. Figure 17 represents the comparison of six switching signals for a two-level three-phase inverter, achieved for horizon N = 2 and modified horizon N = 2. Figure 17A illustrates switching pules given to the inverter in the case of the horizon N = 2, as also discussed in Figure 6. Moreover, Figure 17B shows the switching pulses for the modified horizon N = 2, which is conceptually represented in Figure 6C. This indicates that switching

frequency is reduced, in the case of the proposed control approach. The reduced switching frequency means low switching power loss. Hence, the proposed control approach has less switching frequency than classical MPC schemes.

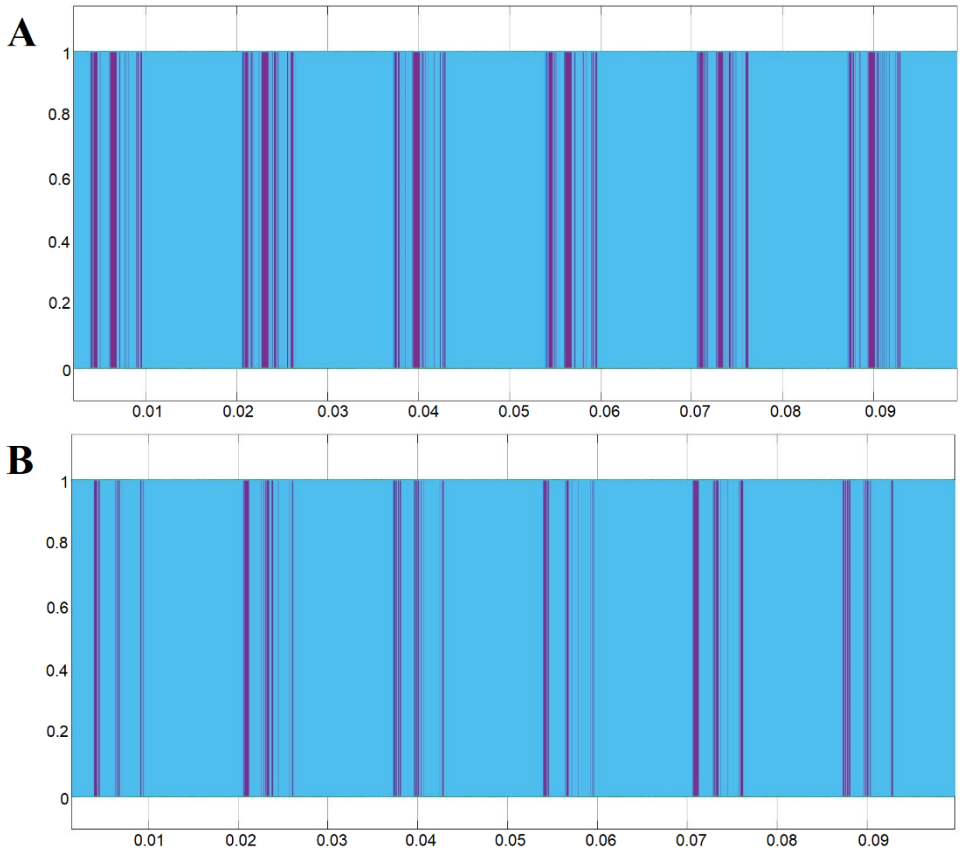


**Figure 17.** Representation of switching signals. (**A**) For horizon N = 2 and (**B**) for modified horizon N = 2.

The main concern about MPC is its variable switching frequency, which causes high switching losses. Usually, a higher switching frequency leads to a higher switching power loss as well as a higher computational burden. The average switching power loss $P_{sw}$ can be calculated as

$$P_{sw} = f_{sw} * \left( E_{sw,on} + E_{sw,off} \right) \tag{31}$$

and computational burden $C_B$ can be represented as

$$C_B \propto f_{sw} \tag{32}$$

According to [54], the optimal switching time $T_{sw}$ for the $k+1$ horizon is represented as

$$T_{sw} = t_{a(k+1)} \tag{33}$$

so, the optimal switching time $T_{sw}$ for the two-step horizon prediction is

$$T_{sw} = t_{a(k+2)} = {t_{a(k+1)}}^2 \tag{34}$$

and the optimal switching time $T_{sw}$ for the modified two-step horizon prediction is

$$T_{sw} = t_{a(k+2)} = t_{a(k+1)} \tag{35}$$

where $f_{sw}$ is the switching frequency, $E_{sw,on}$ is the switching energy loss during the turn-on transition time, and $E_{sw,off}$ is the switching energy loss during the turn-off transition time.

Equation (31) shows that the average switching loss $P_{sw}$ is directly proportional to the switching frequency $f_{sw}$. In the case of modified horizon N = 2, the switching frequency is reduced to seven times. As described in Figure 17B, the average switching losses will also reduce, respectively, as well as the computational burden which results in a high computational speed.

The probability of failure-free performance of a necessary function in a specific environment during a certain period is defined as reliability. The converter's performance relies on the converter's burden due to switching frequency. Reducing switching frequency results in lesser losses, better performance, and thus a reliable system.

### *4.4. Stability and Performance*

In MATLAB/Simulink, a discrete benchmark model of the previously stated system was developed utilizing the Monte Carlo technique. The results of the simulation validate the model's quality. Figure 18 shows the results of the Monte Carlo stability analysis. Reference values of active and reactive power are linearized with the injected current and injected active and reactive powers. Figure 19 shows the statistical analysis, which explains the correlation, partial correlation, and standardized regression between active and reactive power reference values with the injected current and injected active and reactive powers. The results of the Monte Carlo stability analysis authenticate the stability and performance of the proposed technique.

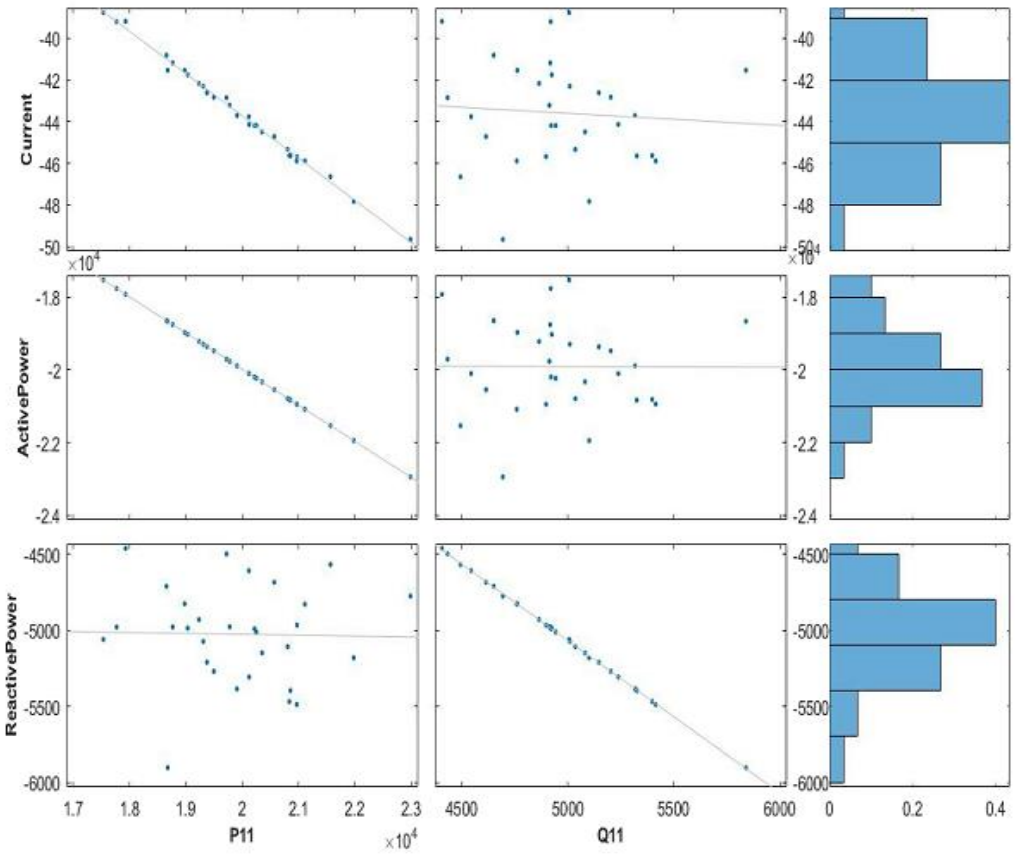


**Figure 18.** Monte Carlo stability analysis of FCS−DPMPC.

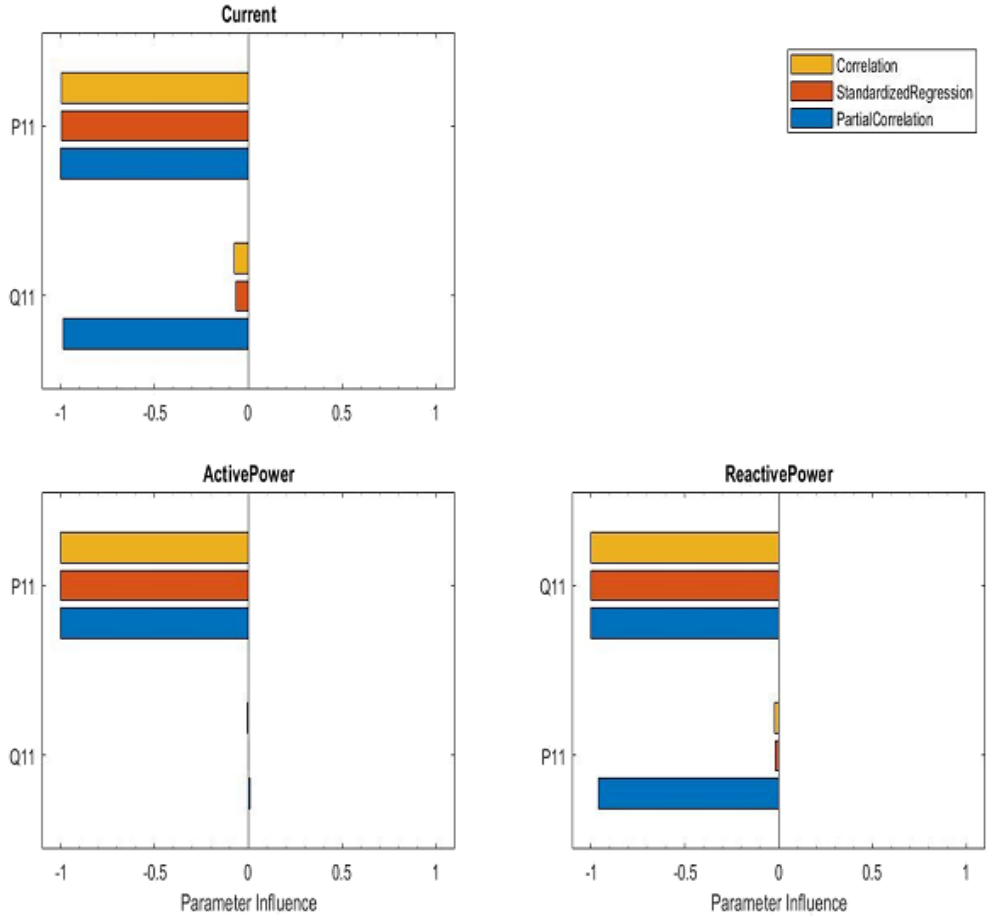


**Figure 19.** Statistics analysis of FCS-DPMPC.

### *4.5. Comparison between Different Techniques*

Table 4 compares the proposed finite set direct power model predictive control (FCS-DPMPC) with other techniques that authenticate the proposed control method's efficiency. Table 4 shows the comparison of %THD for the balanced linear load.

**Table 4.** Comparison Table.

| Ref. | Controller | Modulation | Application | %THD |
|---|---|---|---|---|
| [55] | Classic | SWM | DG | 3.6 |
| [56] | Classic | SPWM | DG | 2.92 |
| [57] | Fuzzy | PWM | PV | 4.71 |
| [58] | Classic | PWM | DG | 4.78 |
| [59] | Hysteresis | PWM | General | 3.62 |
| [60] | MPC | SVPWM | Inverter | 2.3 |
| Proposed | Improved FCS-MPC | - | MG, DG | 1.06 |

Improvements and innovations that can be made in this field in the future are a reduction of %THD and the implementation of a double cost function to operate in both islanded and grid-connected modes. Other similar parametric uncertainty tests are out of the scope of this study.

## 5. Conclusions

This paper studies an improved finite control set direct power model predictive control (FCS-DPMPC) approach with excellent steady-state and transient responses. With this approach, a grid-tied DG system can gain power regulation flexibility, reduce switching frequency, and lower the computational burden compared to classic MPC schemes. This controller is simple in implementation and effective in performance. To predict the system outcomes and minimize power error, a cost function is used. Accordingly, there is no need for any proportional-integral regulator, switching table, or any kind of modulator. Simulation outcomes for both single DG in grid-tie mode and parallel operation of DGs in grid-tie mode are given to authenticate the efficiency of the proposed control method. Statistical model checking is used for checking the stability and performance in which results from Monte Carlo algorithms and statistics analysis authenticate the stability and performance of the proposed model.

**Author Contributions:** Conceptualization, A.S. and M.Z.A.B.; methodology, M.Z.A.B.; software, M.Z.A.B.; validation, A.S., S.A. and W.A.; formal analysis, H.S.K.; investigation, A.S.; writing—original draft preparation, M.Z.A.B.; writing—review and editing, W.A.; supervision, A.S.; project administration, S.A. All authors have read and agreed to the published version of the manuscript.

**Funding:** This research received no external funding.

**Institutional Review Board Statement:** Not applicable.

**Informed Consent Statement:** Not applicable.

**Data Availability Statement:** Not applicable.

**Acknowledgments:** The authors of the article appreciate the referees for their valuable suggestions which contributed to improving the paper.

**Conflicts of Interest:** The authors declare no conflict of interest.

## References

1. Abdelrahem, M.; Hackl, C.M.; Kennel, R. Finite Position Set-Phase Locked Loop for Sensorless Control of Direct-Driven Permanent-Magnet Synchronous Generators. *IEEE Trans. Power Electron.* **2017**, *33*, 3097–3105. [CrossRef]
2. Koutroulis, E.; Blaabjerg, F. Overview of maximum power point tracking techniques for photovoltaic energy production systems. *Electr. Power Compon. Syst.* **2015**, *43*, 1329–1351. [CrossRef]
3. Liserre, M.; Cárdenas, R.; Molinas, M.; Rodriguez, J. Overview of multi-MW wind turbines and wind parks. *IEEE Trans. Ind. Electron.* **2011**, *58*, 1081–1095. [CrossRef]
4. Hu, J.; Zhu, J.; Dorrell, D.G.; Guerrero, J.M. Virtual flux droop method—A new control strategy of inverters in microgrids. *IEEE Trans. Power Electron.* **2013**, *29*, 4704–4711. [CrossRef]
5. Hu, J.; Zhu, J.; Platt, G. Smart grid—The next generation electricity grid with power flow optimization and high power quality. In Proceedings of the 2011 International Conference on Electrical Machines and Systems, Beijing, China, 20–23 August 2011.
6. Funde, N.; Dhabu, M.; Deshpande, P. CLOES: Cross-layer optimal energy scheduling mechanism in a smart distributed multi-microgrid system. *J. Ambient. Intell. Humaniz. Comput.* **2020**, *11*, 4765–4783. [CrossRef]
7. Jadav, K.A.; Karkar, H.M.; Trivedi, I. A Review of microgrid architectures and control strategy. *J. Inst. Eng.* **2017**, *98*, 591–598. [CrossRef]
8. Wang, X.; Guerrero, J.M.; Blaabjerg, F.; Chen, Z. Secondary voltage control for harmonics suppression in islanded microgrids. In Proceedings of the 2011 IEEE Power and Energy Society General Meeting, Detroit, MI, USA, 24–28 July 2011.
9. Zhang, Y.; Qu, C. Direct power control of a pulse width modulation rectifier using space vector modulation under unbalanced grid voltages. *IEEE Trans. Power Electron.* **2014**, *30*, 5892–5901. [CrossRef]
10. Jiang, W.; Wang, Y.; Wang, J.; Wang, L.; Huang, H. Maximizing instantaneous active power capability for PWM rectifier under unbalanced grid voltage dips considering the limitation of phase current. *IEEE Trans. Ind. Electron.* **2016**, *63*, 5998–6009. [CrossRef]
11. Sun, D.; Wang, X. Low-complexity model predictive direct power control for DFIG under both balanced and unbalanced grid conditions. *IEEE Trans. Ind. Electron.* **2016**, *63*, 5186–5196. [CrossRef]
12. Wang, X.; Sun, D.; Zhu, Z.Q. Resonant-based backstepping direct power control strategy for DFIG under both balanced and unbalanced grid conditions. *IEEE Trans. Ind. Appl.* **2017**, *53*, 4821–4830. [CrossRef]
13. Khan, H.S.; Aamir, M.; Ali, M.; Waqar, A.; Ali, S.U.; Imtiaz, J. Finite control set model predictive control for parallel connected online ups system under unbalanced and nonlinear loads. *Energies* **2019**, *12*, 581. [CrossRef]

14. Khan, H.S.; Aamir, M.; Kauhaniemi, K.; Mumtaz, M.; Hassan, M.W.; Ali, M. Improved finite control set model predictive control for distributed energy resource in islanded microgrid with fault-tolerance capability. *Eng. Sci. Technol. Int. J.* **2021**, *24*, 694–705. [CrossRef]
15. Liu, T.; Chen, A.; Qin, C.; Chen, J.; Li, X. Double vector model predictive control to reduce common-mode voltage without weighting factors for three-level inverters. *IEEE Trans. Ind. Electron.* **2020**, *67*, 8980–8990. [CrossRef]
16. Alsofyani, I.M.; Lee, K.B. Three-level inverter-fed model predictive torque control of a permanent magnet synchronous motor with discrete space vector modulation and simplified neutral point voltage balancing. *J. Power Electron.* **2022**, *22*, 22–30. [CrossRef]
17. Jayan, V.; Ghias, A.M.Y.M.; Guerrero, J.M.; Merabet, M. An Adaptive Dynamic Reference Control for Power Converters in a Microgrid. *IEEE Trans. Power Electron.* **2022**, *37*, 9164–9174. [CrossRef]
18. Liu, T.; Chen, A.; Gao, F.; Liu, X.; Li, X.; Hu, S. Double-Loop Control Strategy with Cascaded Model Predictive Control to Improve Frequency Regulation for Islanded Microgrids. *IEEE Trans. Smart Grid* **2021**, *13*, 3954–3967. [CrossRef]
19. Hong, J.; Zhang, X.; Cao, R. Robust model predictive control for three-level voltage source inverters. *J. Power Electron.* **2021**, *21*, 747–756. [CrossRef]
20. Preindl, M.; Schaltz, E.; Thogersen, P. Switching frequency reduction using model predictive direct current control for high-power voltage source inverters. *IEEE Trans. Ind. Electron.* **2010**, *58*, 2826–2835. [CrossRef]
21. Roh, C.; Kwak, S.; Choi, S. Three-phase three-level four-leg NPC converters with advanced model predictive control. *J. Power Electron.* **2021**, *21*, 1574–1584. [CrossRef]
22. Vu, H.-C.; Lee, H.-H. Simplified model predictive current control strategy for dual five-phase VSI-fed open end load to eliminate common-mode voltage and reduce current harmonics. *J. Power Electron.* **2021**, *21*, 1155–1165. [CrossRef]
23. Abdelrahem, M.; Hackl, C.M.; Zhang, Z.; Kannel, R. Robust predictive control for direct-driven surface-mounted permanent-magnet synchronous generators without mechanical sensors. *IEEE Trans. Energy Convers.* **2017**, *33*, 179–189. [CrossRef]
24. Mohamed, Y.A.-R.I.; El-Saadany, E.F. Robust high bandwidth discrete-time predictive current control with predictive internal model—A unified approach for voltage-source PWM converters. *IEEE Trans. Power Electron.* **2008**, *23*, 126–136. [CrossRef]
25. Hackl, C.M. MPC with analytical solution and integral error feedback for LTI MIMO systems and its application to current control of grid-connected power converters with LCL-filter. In Proceedings of the 2015 IEEE International Symposium on Predictive Control of Electrical Drives and Power Electronics (PRECEDE), Valparaiso, Chile, 5–6 October 2015.
26. Quevedo, D.E.; Aguilera, R.P.; Geyer, T. Predictive control in power electronics and drives: Basic concepts, theory, and methods. In *Advanced and Intelligent Control in Power Electronics and Drives*; Springer: New York, NY, USA, 2014; pp. 181–226.
27. Abdelrahem, M.; Kennel, R. Fault-ride through strategy for permanent-magnet synchronous generators in variable-speed wind turbines. *Energies* **2016**, *9*, 1066. [CrossRef]
28. Abdelrahem, M.; Kennel, R. Efficient direct model predictive control for doubly-fed induction generators. *Electr. Power Compon. Syst.* **2017**, *45*, 574–587. [CrossRef]
29. Khan, H.S.; Kumar, J.; Kauhaniemi, K. Design and Implementation of Model Predictive Control for Parallel Distributed Energy Resource in Islanded AC Microgrids. In Proceedings of the 2021 6th IEEE Workshop on the Electronic Grid (eGRID), New Orleans, LA, USA, 8–10 November 2021; pp. 1–7. [CrossRef]
30. Sangsefidi, Y.; Ziaeinejad, S.; Mehrizi-Sani, A. Low switching frequency-based predictive control of a grid-connected voltage-sourced converter. *IEEE Trans. Energy Convers.* **2016**, *32*, 686–697. [CrossRef]
31. Abdelrahem, M.; Hamadto, F.; Garikapati, A.; Kennel, R.; Rodriguez, J. Multiple-vector direct model predictive control for grid-connected power converters with reduced calculation burden. In Proceedings of the 2019 IEEE International Symposium on Predictive Control of Electrical Drives and Power Electronics (PRECEDE), Quanzhou, China, 31 May–2 June 2019.
32. Kang, S.-W.; Soh, J.-H.; Kim, R.-Y. Symmetrical three-vector-based model predictive control with deadbeat solution for IPMSM in rotating reference frame. *IEEE Trans. Ind. Electron.* **2019**, *67*, 159–168. [CrossRef]
33. Tarisciotti, L.; Zanchetta, P.; Watson, A.; Clare, J.C.; Degano, M.; Bifaretti, S. Modulated model predictive control for a three-phase active rectifier. *IEEE Trans. Ind. Appl.* **2014**, *51*, 1610–1620. [CrossRef]
34. Kwak, S.; Park, J.-C. Switching strategy based on model predictive control of VSI to obtain high efficiency and balanced loss distribution. *IEEE Trans. Power Electron.* **2013**, *29*, 4551–4567. [CrossRef]
35. Khan, H.S.; Mohamed, I.S.; Kauhaniemi, K.; Liu, L. Artificial neural network-based voltage control of DC/DC converter for dc microgrid applications. In Proceedings of the 2021 6th IEEE Workshop on the Electronic Grid (eGRID), New Orleans, LA, USA, 8–10 November 2021; pp. 1–6.
36. Böcker, J.; Mohamed, I.S.; Kauhaniemi, K.; Liu, L. Experimental comparison of model predictive control and cascaded control of the modular multilevel converter. *IEEE Trans. Power Electron.* **2014**, *30*, 422–430. [CrossRef]
37. Wang, Y.; Wang, X.; Xie, W.; Wang, F.; Dou, M.; Kennel, R.M.; Lorenz, R.D.; Gerling, D. Deadbeat model-predictive torque control with discrete space-vector modulation for PMSM drives. *IEEE Trans. Ind. Electron.* **2017**, *64*, 3537–3547. [CrossRef]
38. Luo, Y.; Liu, C.; Yu, F. Predictive current control of a new three-phase voltage source inverter with phase shift compensation. *IET Electr. Power Appl.* **2017**, *11*, 740–748. [CrossRef]
39. Zhang, Y.; Peng, Y.; Yang, H. Performance improvement of two-vectors-based model predictive control of PWM rectifier. *IEEE Trans. Power Electron.* **2015**, *31*, 6016–6030. [CrossRef]
40. Cortes, P.; Rodriguez, J.; Silva, C.; Flores, A. Delay Compensation in Model Predictive Current Control of a Three-Phase Inverter. *IEEE Trans. Ind. Electron.* **2012**, *59*, 1323–1325. [CrossRef]

41. Rawlings, J.; Mayne, D. *Model Predictive Control: Theory and Design*; Nob Hill: Santa Barbara, CA, USA, 2009.
42. Yaramasu, V.; Wu, B. *Model Predictive Control of Wind Energy Conversion Systems*; IEEE Press Series on Power Engineering; Wiley: Hoboken, NJ, USA, 2016.
43. Vazquez, S.; Leon, J.I.; Franquelo, L.G.; Rodriguez, J.; Young, H.A.; Marquez, A.; Zanchetta, P. Model predictive control: A review of its applications in power electronics. *IEEE Ind. Electron. Mag.* **2014**, *8*, 16–31. [CrossRef]
44. Fard, R.N.; Nademi, H.; Norum, L. Analysis of a modular multilevel inverter under the predicted current control based on finite-control-set strategy. In Proceedings of the 2013 3rd International Conference on Electric Power and Energy Conversion Systems EPECS, Istanbul, Turkey, 2–4 October 2013; pp. 1–6.
45. Yaramasu, V.; Rivera, M.; Wu, B.; Rodriguez, J. Model predictive current control of two-level four-leg inverters;part i: Concept, algorithm, and simulation analysis. *IEEE Trans. Power Electron.* **2013**, *28*, 3459–3468. [CrossRef]
46. Young, H.A.; Perez, M.A.; Rodriguez, J.; Abu-Rub, H. Assessing finite-control-set model predictive control: A comparison with a linear current controller in two-level voltage source inverters. *IEEE Ind. Electron. Mag.* **2014**, *8*, 44–52. [CrossRef]
47. Aguilera, R.P.; Quevedo, D.E. Predictive control of power converters: Designs with guaranteed performance. *IEEE Trans. Ind. Inform.* **2015**, *11*, 53–63. [CrossRef]
48. Aguilera, R.P.; Quevedo, D.E. On stability and performance of finite control set MPC for power converters. In Proceedings of the 2011 Workshop on Predictive Control of Electrical Drives and Power Electronics, Munich, Germany, 14–15 October 2011; pp. 55–62.
49. Aguilera, R.P.; Quevedo, D.E. On stability of finite control set MPC strategy for multicell converters. In Proceedings of the 2010 IEEE International Conference on Industrial Technology, Via del Mar, Chile, 14–17 May 2010; pp. 1277–1282.
50. Akter, P.; Mekhilef, S.; Tan, N.M.L.; Akagi, H. Modified model predictive control of a bidirectional AC-DC converter based on lyapunov function for energy storage systems. *IEEE Trans. Ind. Electron.* **2016**, *63*, 704–715. [CrossRef]
51. Boudjadar, A.; David, A.; Kim, J.H.; Larsen, K.G.; Mikučionis, M.; Nyman, U.; Skou, A. Statistical and exact schedulability analysis of hierarchical scheduling systems. *Sci. Comput. Program.* **2016**, *127*, 103–130. [CrossRef]
52. Larsen, K.G.; Mikučionis, M.; Muñiz, M.; Srba, J.; Taankvist, J.H. Online and compositional learning of controllers with application to floor heating. In *Tools and Algorithms for the Construction and Analysis of Systems, Proceedings of the International Conference on Tools and Algorithms for the Construction and Analysis of Systems, Eindhoven, The Netherlands, 2–8 April 2016*; Springer: New York, NY, USA, 2016.
53. Larsen, K.G.; Legay, A. On the power of statistical model checking. In *International Symposium on Leveraging Applications of Formal Methods*; Springer: New York, NY, USA, 2016.
54. Hu, B.; Kang, L.; Liu, J.; Zeng, J.; Wang, S.; Zhang, Z. Model Predictive Direct Power Control with Fixed Switching Frequency and Computational Amount Reduction. *IEEE J. Emerg. Sel. Top. Power Electron.* **2019**, *7*, 956–966. [CrossRef]
55. Liu, Z.; Liu, J.; Zhao, Y. A unified control strategy for three-phase inverter in distributed generation. *IEEE Trans. Power Electron.* **2013**, *29*, 1176–1191.
56. Li, Y.; Jiang, S.; Cintron-Rivera, J.G.; Peng, F.Z. Modeling and control of quasi-Z-source inverter for distributed generation applications. *IEEE Trans. Ind. Electron.* **2012**, *60*, 1532–1541. [CrossRef]
57. Ouchen, S.; Betka, A.; Abdeddaim, S.; Menadi, A. Fuzzy-predictive direct power control implementation of a grid connected photovoltaic system, associated with an active power filter. *Energy Convers. Manag.* **2016**, *122*, 515–525. [CrossRef]
58. Chilipi, R.; Sayari, N.A.; Al Hosani, K.; Beig, A.B. Control scheme for grid-tied distributed generation inverter under unbalanced and distorted utility conditions with power quality ancillary services. *IET Renew. Power Gener.* **2016**, *10*, 140–149. [CrossRef]
59. Zhang, X.; Wang, Y.; Yu, C.; Guo, L.; Cao, R. Hysteresis model predictive control for high-power grid-connected inverters with output LCL filter. *IEEE Trans. Ind. Electron.* **2016**, *63*, 246–256. [CrossRef]
60. Zhang, X.; Tan, L.; Xian, J.; Zhang, H.; Ma, Z.; Kang, J. Direct grid-side current model predictive control for grid-connected inverter with LCL filter. *IET Power Electron.* **2018**, *11*, 2450–2460. [CrossRef]